Chemical Engineering Journal 475 (2023) 146266

Contents lists available at ScienceDirect

Chemical Engineering Journal

journal homepage: www.elsevier.com/locate/cej

Dual-type gel polymer electrolyte for high-voltage lithium metal batteries with excellent cycle life

A-Hyeon Ban [a], Su-Jin Pyo [a], Woo Jin Bae [b], Hyun-Sik Woo [b], Jongseok Moon [b], Dong-Won Kim [a,c,*]

[a] Department of Chemical Engineering, Hanyang University, Seoul 04763, Republic of Korea
[b] SDI R&D Center, Samsung SDI, Gyeonggi-do 16678, Republic of Korea
[c] Department of Battery Engineering, Hanyang University, Seoul 04763, Republic of Korea

ARTICLE INFO

Keywords:
Lithium metal battery
High-voltage cathode
Gel polymer electrolytes
Dual-type electrolyte
In-situ cross-linking
High energy density

ABSTRACT

The most attractive approach for maximizing the energy density of rechargeable lithium batteries is to combine a lithium metal anode with a high-voltage cathode. However, the dendritic formation of lithium at the anode and the highly oxidizing conditions that cause electrolyte decomposition at the cathode have hindered the practical development of lithium metal batteries (LMBs). In this study, we report a dual-type gel polymer electrolyte (GPE) composed of an anolyte and a catholyte that can address the drawbacks of both the anode and cathode sides. The anolyte is a poly(ethylene oxide)-based composite solid polymer electrolyte that is chemically stable with lithium metal and has a high mechanical strength for suppressing lithium dendrite growth. A cross-linked gel polymer electrolyte with high lithium-ion conductivity and oxidative stability was used as the catholyte. The Li/$LiCoO_2$ cell assembled with a dual-type GPE exhibited a high discharge capacity of 181.1 mAh g^{-1} (areal capacity: 3.15 mAh cm^{-2}) in the voltage range of 3.0–4.5 V and excellent cycle life, with a capacity retention of 74 % after 700 cycles at 25 °C and 0.5 C rate. Our study proposes a promising electrolyte system for LMBs with high energy density and good cycle life.

1. Introduction

As the energy density of lithium-ion batteries (LIBs) is limited, the battery market is prompting the development of ultra-high energy density lithium batteries [1–3]. One of the most promising approaches to increase the energy density of batteries is to couple a lithium metal anode with high-voltage cathodes, such as $LiCoO_2$ (LCO), $LiNi_{0.5}Mn_{1.5}O_4$, and Ni-rich layered oxides ($LiNi_xCo_yMn_{1-x-y}O_2$, $x \geq 0.6$) [4–6]. However, the development of lithium metal batteries (LMBs) operating at high voltages has been hindered by the severe side reactions of carbonate-based liquid electrolytes with both lithium metal anodes and high-voltage cathodes. Carbonate solvents undergo oxidative decomposition at high voltages (>4.3 V vs. Li/Li^+), forming a thick and resistive passivation layer on the cathode surface [7,8]. On the anode side, lithium metal suffers from deleterious side reactions with the liquid electrolyte, resulting in the formation of an inhomogeneous solid-electrolyte interphase (SEI). The unstable SEI is continuously destroyed and reformed during charge–discharge cycles, leading to low coulombic efficiency and lithium dendrite growth, which cause large capacity fading and safety problems in LMBs [9–12].

Given the high reactivity of lithium metal with carbonate-based liquid electrolytes, various studies have been conducted to improve the cycling performance of LMBs employing liquid electrolytes, such as ether-based electrolytes [13,14], high-concentration electrolytes (HCEs) [15,16], and localized high-concentration electrolytes (LHCEs) [17,18]. Although ether-based electrolytes are compatible with lithium anodes, they have been excluded from use in high-voltage LMBs because of their low anodic stability [7]. HCEs and LHCEs can be good alternatives to improve oxidative stability; however, they are not appropriate for practical applications due to the high cost of large amounts of lithium salts and fluorinated solvents [19,20]. As such, the development of carbonate-based liquid electrolytes with good compatibility with lithium anodes has significant value in practical applications. Dahn et al. reported a dual-salt liquid electrolyte for anode-free LMBs with long cycle life and dendrite-free lithium morphology [21]. Another approach is to use chemically stable gel polymer electrolytes (GPEs) [22–24],

* Corresponding author at: Department of Chemical Engineering, Hanyang University, Seoul 04763, Republic of Korea.
E-mail address: dongwonkim@hanyang.ac.kr (D.-W. Kim).

https://doi.org/10.1016/j.cej.2023.146266
Received 1 July 2023; Received in revised form 28 August 2023; Accepted 23 September 2023
Available online 25 September 2023

which possess both advantageous characteristics of liquid and solid polymer electrolytes, such as high ionic conductivity, good interfacial contact with electrodes, and good film formability. The polymer matrix in GPE effectively encapsulates organic solvents and suppresses side reactions with the electrodes [25,26]. Moreover, incorporating inorganic fillers into polymer electrolytes improves the mechanical properties and ionic conductivity of GPEs [27–30]. Recently, high-concentration poly(ethylene oxide)(PEO)-based solid polymer electrolyte with high oxidative and interfacial stabilities was applied to lithium metal batteries, and their stable cycling performance was reported at 60 °C [31].

In this study, we developed a dual-type GPE that combines advantages of composite solid polymer electrolyte and gel polymer electrolyte. A poly(ethylene oxide) (PEO)-based composite solid polymer electrolyte used as an anolyte was inspired by our previous work on improving the mechanical properties of polymer electrolytes using functionalized inorganic fillers as cross-linkers [32,33]. A three-dimensional cross-linked network structure induced by a thermal cross-linking reaction using reactive alumina provides additional mechanical strength to the anolyte, inhibiting lithium dendrite growth during the repeated cycling. A cross-linked GPE catholyte was synthesized via the *in-situ* thermal curing of a dual-salt liquid electrolyte using a cross-linking agent. The oxidative decomposition of liquid electrolyte in the GPE was suppressed by effectively trapping the organic solvents in the cross-linked polymer networks. Due to the synergistic effect of the anolyte and catholyte, the dual-type GPE suppressed the side reactions at both the lithium metal anode and high-voltage cathode and the dendritic growth of lithium on the anode side. As a result, the Li/$LiCoO_2$ cell (areal capacity: 3.15 mAh cm^{-2}) employing the dual-type GPE exhibited a superior capacity retention of 74 % after 700 cycles in the voltage range of 3.0–4.5 V at 0.5 C rate and 25 °C.

2. Experimental section

2.1. Materials

PEO (M_w: 300,000) was obtained from Sigma-Aldrich and vacuum dried at 50 °C for 12 h. Pentaerythritol tetraacrylate (PETTA, Sigma-Aldrich), divinyl benzene (DVB, Sigma-Aldrich), and *tert*-butyl peroxypivalate (t-BPP, Arkema) were used after dehydrating with 4 Å molecular sieves. Single lithium-ion conducting monomers, that is, lithium sulfonyl(trifluoromethane sulfonyl)imide methacrylate (MTFSILi) and lithium sulfonyl(trifluoromethane sulfonyl)imide styrene (STFSILi) were obtained from Specific Polymers. Reactive alumina (AEROXIDE® Alu C 711; Evonik) was vacuum dried before use at 80 °C for 12 h. It has 3-methacryloxy propyl trimethoxysilane on its surface. Fig. S1 shows the chemical structures of PETTA, MTFSILi, STFSILi, and reactive alumina. $Li_{6.4}La_{3.0}Zr_{1.4}Ta_{0.6}O_{12}$ (LLZTO, > 99.99 %, d_{50}: 400 nm, MTI), tetrahydrofuran (THF, > 99.5 %, TCI), lithium bis(trifluoromethanesulfonyl) imide (LiTFSI, Dongwha Electrolyte) were used as received. A polyethylene (PE) separator (20 μm, Toray) was used after vacuum drying at 70 °C. The dual-salt liquid electrolyte composed of 0.6 M of lithium tetrafluoroborate ($LiBF_4$) and 0.6 M of lithium difluoro(oxalato)borate (LiDFOB) in a mixture of diethyl carbonate (DEC) and fluoroethylene carbonate (FEC) (2:1, by volume) was kindly supplied from Dongwha Electrolyte Co. Ltd.

2.2. Preparation of the anolyte and catholyte

The anolyte was prepared using a solution-casting method. To prepare the precursor solution, PEO, LiTFSI, STFSILi, DVB, reactive alumina, and LLZTO were mixed at a weight ratio of 36: 18: 10: 6: 5: 25, respectively, in anhydrous THF. t-BPP was added into the solution as an initiator. The precursor solution was cast using a doctor blade onto the lithium foil (thickness 100 μm, Honjo Metal Co. Ltd.) laminated on a Cu current collector, and the solvent was left to evaporate slowly at 70 °C under an inert atmosphere. Finally, the anolyte was thermally cured in a vacuum oven at 70 °C for 12 h, forming a PEO-based composite solid

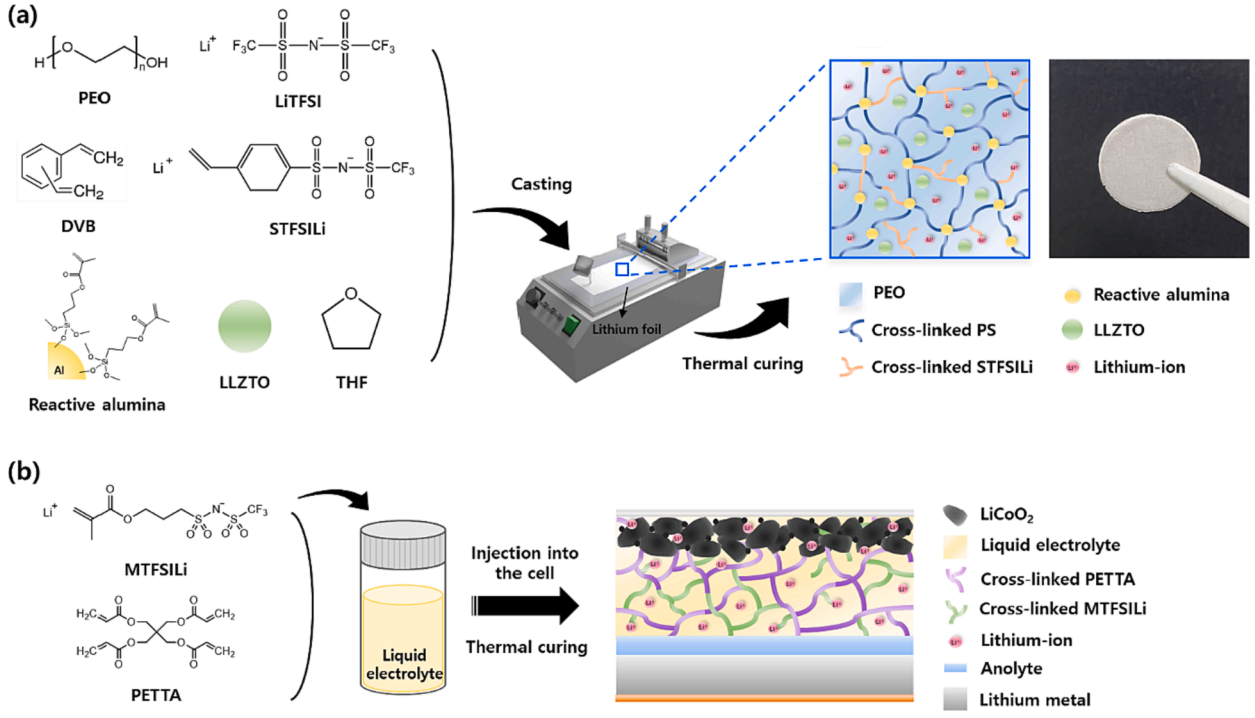

Fig. 1. Schematic presentation of the preparation of the dual-type GPE and the LMB featuring the dual-type GPE. (a) Anolyte synthesized onto the lithium metal anode, and (b) catholyte and LMB assembled with dual-type GPE.

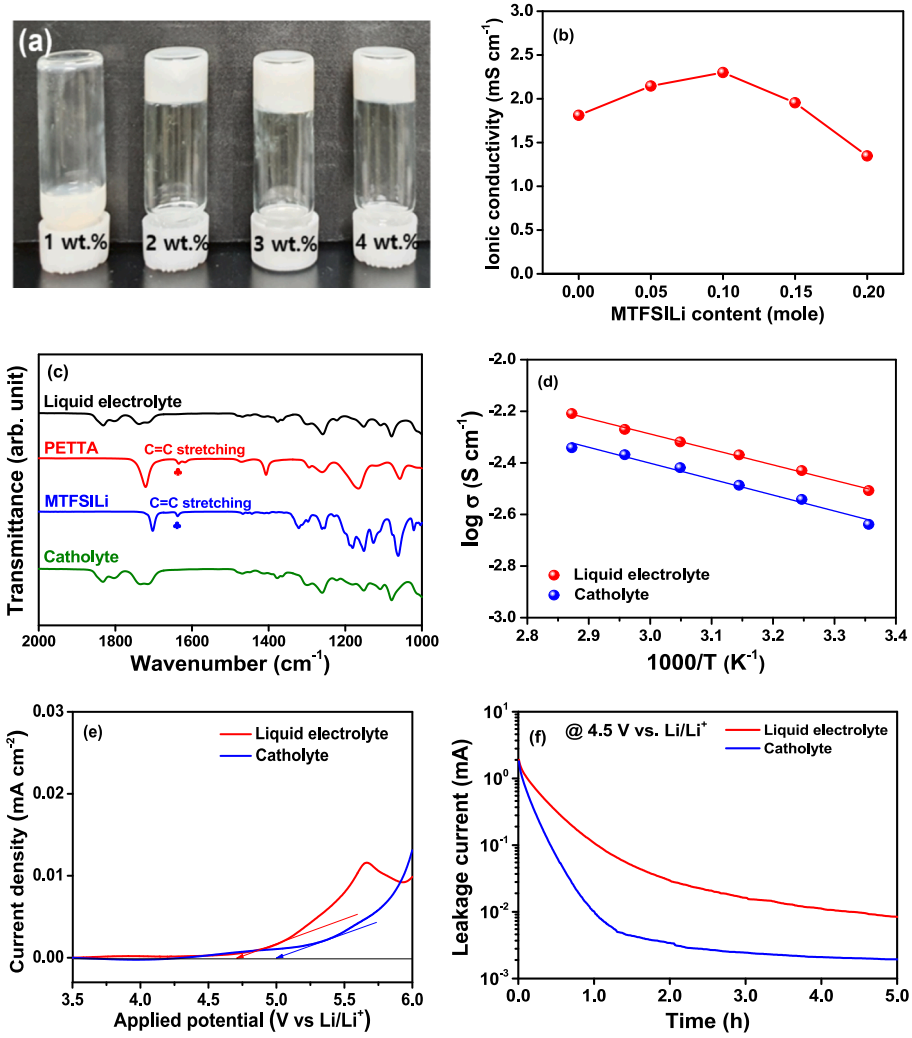

Fig. 2. (a) Image of catholytes cured with different amounts of PETTA. (b) Ionic conductivities of catholytes as a function of MTFSILi content. (c) FT-IR spectra of liquid electrolyte, PETTA, MTFSILi, and catholyte. (d) Temperature dependence of the ionic conductivities of the liquid electrolyte and catholyte. (e) Linear sweep voltammograms of liquid electrolyte and catholyte at 25 °C. (f) Leakage current of the Li/LCO cells with liquid electrolyte and catholyte at 4.5 V.

electrolyte on the lithium metal. The catholyte was prepared via *in-situ* thermal curing. The catholyte precursor consisted of a cross-linking agent (PETTA, 1.0 ~ 4.0 wt.%), single lithium-ion conducting monomer (MTFSILi, 0.1 ~ 0.2 mol), liquid electrolyte (96 ~ 99 wt.%), and a thermal initiator (t-BPP, 1.0 wt.% of monomers). After injecting the catholyte precursor into the Li/$LiCoO_2$ cell, the cell was kept at 70 °C for 1.5 h to drive the cross-linking reaction and obtain the cross-linked GPE as a catholyte.

2.3. Electrode preparation and cell assembly

The LCO cathode coated on an aluminum current collector was provided by Samsung SDI. The content of active material in the cathode was 97.5 wt.%, and its mass loading was approximately 17.4 mg cm^{-2}. The Li/LCO cell was assembled by stacking an anolyte-coated lithium anode, a PE separator, and an LCO cathode in a CR2032-type coin cell. The catholyte precursor was then injected into the cell and thermally cured at 70 °C for 1.5 h in the cell, finally forming the dual-type GPE. All cells were assembled in an Ar-gas-filled glove box.

2.4. Electrochemical measurements

A stainless-steel symmetric cell with an electrolyte was assembled. Electrochemical impedance spectroscopy (EIS) was performed to measure the ionic conductivity at different temperatures in the frequency range of 10 Hz – 1 MHz using an impedance analyzer (ZIVE MP1, Wonatech). The lithium-ion transference number (t^+) in the electrolyte was measured in the symmetrical Li/electrolyte/Li cell using a combination of AC impedance and DC polarization measurements at 25 °C [34]. Linear sweep voltammetry (LSV) was performed at a scan rate of 1 mV s^{-1} using a CHI 660 analyzer (CH Instruments, Inc.). The leakage current was measured in the Li/LCO cell charged at 4.5 V and held at 4.5 V for 5 h [35]. A galvanostatic cycling test of the Li/LCO cell was conducted in the voltage range of 3.0–4.5 V at 25 °C with a battery tester (WBCS 3000, Wonatech). During pre-conditioning cycle of the cell, it was charged and discharged at a 0.1 C rate for one cycle. After the pre-conditioning cycle, the cell was charged and discharged at 0.2 C and 0.5 C rates, respectively.

2.5. Characterization

Fourier transform infrared (FT-IR) spectroscopy was performed to confirm the cross-linking reaction of the electrolytes using a Nicolet iS50 spectrometer. The morphologies of the lithium anode and anolyte were characterized using field-emission scanning electron microscopy (FE-SEM; Verios G4UC, FEI). The chemical composition of the surface layer formed on the electrodes was investigated using X-ray photoelectron spectroscopy (XPS; K-alpha$^+$, Thermo Fisher Scientific). ^1H and ^{19}F

nuclear magnetic resonance (NMR) analyses were performed using a VNMRS 600 MHz spectrometer (Agilent Technologies). Dimethylsulfoxide-d_6 (DMSO-d_6, >99.9 %, Cambridge Isotope) was used as the solvent, with tetramethylsilane as a reference. All cell components were transferred to a vial containing 1 mL of DMSO-d_6 and 1 mg of dimethyl carbonate as an inert marker. They were mixed using a vortex mixer for 1 min and filtered through a polytetrafluoroethylene membrane. The filtered mixture was collected for NMR analysis. Mechanical property of anolyte and different solid electrolytes was evaluated by using a universal testing machine (UTM, Instron 34SC-1).

3. Results and discussion

Fig. 1a shows a schematic representation of the preparation of the dual-type GPE (anolyte and catholyte) and the LMB featuring the dual-type GPE. The anolyte is a solid-state composite electrolyte with a semi-interpenetrating polymer network (semi-IPN) composed of linear PEO and a cross-linked polymer. A three-dimensional cross-linked structure consisting of reactive alumina and polystyrene network induced by DVB provides mechanical strength to the anolyte. In the anolyte, both PEO/LiTFSI and poly(STFSILi)(single lithium ion-conducting polymer) facilitate the transport of lithium ions at the surface of the lithium anode, enabling the uniform deposition and stripping of lithium during the repeated cycling. To further enhance the ionic conductivity and mechanical strength of the anolyte, LLZTO particles were incorporated as the Li^+-ion-conductive inorganic fillers. The mechanical strength of anolyte was measured based on the stress–strain curves using universal testing machine, and the results are shown in Fig. S2. For comparison purposes, we prepared two different solid electrolytes; PEO-LiTFSI ([EO]:[LiTFSI] = 10:1) and PEO-LiTFSI-LLZTO (25 wt.% LLZTO). As can be seen in figure, the anolyte exhibited the highest tensile strength and modulus among the solid electrolytes investigated. In addition to the strong mechanical strength of inorganic LLZTO particles, the three-dimensional network structure formed by thermal curing of reactive alumina, DVB and STFSILi contributed to the enhancement of mechanical strength of anolyte. The enhanced mechanical strength of the anolyte are expected to effectively suppress the growth of lithium dendrite [30,36,37]. The catholyte was synthesized by the *in-situ* thermal curing of a precursor solution containing a dual-salt liquid electrolyte, MTFSILi, and PETTA as a cross-linking agent. The cross-linked structure derived from PETTA allows the encapsulation of the liquid electrolyte and improves the oxidative stability of the catholyte. Poly(MTFSILi) can supply additional lithium ions and increase the chain flexibility of the cross-linked polymer networks. The Li/LCO cell was fabricated by combining the anolyte and catholyte, as shown in Fig. 1b.

Fig. 2a shows a photographic image of the catholytes cured with different amounts of PETTA. Catholytes synthesized with PETTA contents higher than 2 wt.% became non-fluidic gel, forming a cross-linked network polymer that effectively encapsulates the liquid electrolyte. The ionic conductivity of the catholyte was measured as a function of the PETTA content, and the results are shown in Fig. S3. As predicted, the ionic conductivity decreased with increasing PETTA content, because the polymer network with a high degree of cross-linking lowered the ionic mobility. The catholyte synthesized with 2 wt.% PETTA exhibited an ionic conductivity of 1.8 mS cm^{-1}, which was lower than that of the liquid electrolyte (3.2 mS cm^{-1}). To compensate for the lower ionic conductivity of the catholyte synthesized with 2 wt.% PETTA, we added a small amount of MTFSILi in the catholyte precursor. Fig. 2b shows the ionic conductivities of the catholytes as functions of the additional MTFSILi content. Ionic conductivity increased with MTFSILi content and reached a maximum of 2.3 mS cm^{-1} at 0.1 mol of MTFSILi. This result can be attributed to two conflicting effects on the ionic conductivity. At low MTFSILi content, the number of lithium ions increases with increasing MTFSILi content. However, the ionic mobility decreases with a further increase in the MTFSILi content due to the increase in the polymer content of the catholyte, consequently decreasing ionic

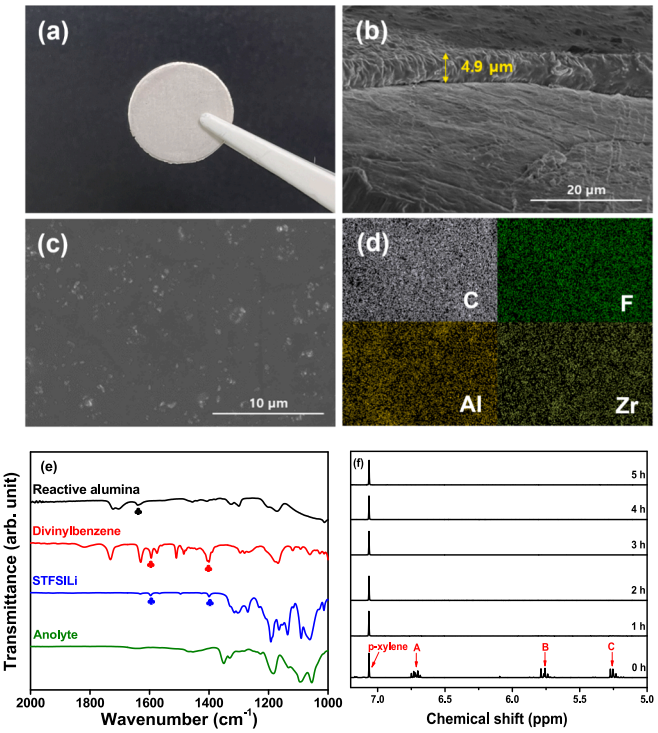

Fig. 3. (a) Image of anolyte synthesized on lithium metal. (b) Cross-sectional, (c) surface, and (d) corresponding EDS mapping images of the anolyte. (e) FT-IR spectra of reactive alumina, divinylbenzene, STFSILi, and anolyte. The symbols (♣) correspond the stretching vibration of C = C bond. (f) ^{1}H NMR spectra of precursor and anolytes with different curing time at 70 °C.

conductivity. Thus, the MTFSILi content was optimized to be 0.1 mol in synthesizing the catholyte. FT-IR analysis was performed to confirm the cross-linking reaction between PETTA and MTFSILi in the presence of the liquid electrolyte (Fig. 2c). The peak observed at 1636 cm^{-1} corresponds to the C = C stretching vibrations of PETTA and MTFSILi [38]. In the FT-IR spectrum of the catholyte synthesized by the thermal curing of PETTA and MTFSILi, the peak associated with the C = C double bonds disappeared, indicating that both PETTA and MTFSILi participated in free radical polymerization, resulting in the formation of the cross-linked polymer. The temperature dependences of the ionic conductivities of the catholyte and liquid electrolyte are compared in Fig. 2d. The activation energy (E_a) for ion conduction in the electrolyte was estimated from the Arrhenius plot [39]. The catholyte had an E_a value (5.28 kJ mol^{-1}) similar to that of the liquid electrolyte (5.12 kJ mol^{-1}), despite its non-fluidity. This can be ascribed to the high concentration of Li^+ ions dissociated from poly(MTFSILi). Moreover, polyester chains derived from PETTA could solvate lithium salts and transport lithium ions via local segmental motion [40]. To investigate the transport of Li^+ ions dissociated from poly(MTFSILi), the lithium-ion transference number (t^+) was measured using a combination of AC impedance and DC polarization experiments (Fig. S4). As shown in Table S1, the catholyte had a t^+ value of 0.33, which is higher than that of the liquid electrolyte (0.25). A lithium-ion conductivity (σ_{Li+}) was obtained by multiplying the lithium-ion transference number (t^+) by ionic conductivity (σ). The lithium-ion conductivity of the catholyte was approximately the same as that of the liquid electrolyte, which can be attributed to the incorporation of a single lithium-ion-conducting poly(MTFSILi). LSV examined the electrochemical stability of the electrolytes, and the results are shown in Fig. 2e. The anodic current showed an abrupt rise at approximately 4.7 V vs. Li/Li^+ in the liquid electrolyte, which can be ascribed to the oxidative decomposition of the electrolyte [41]. In contrast, the catholyte exhibited superior oxidative stability higher than 5.0 V, demonstrating that the cross-linked polymer network in the

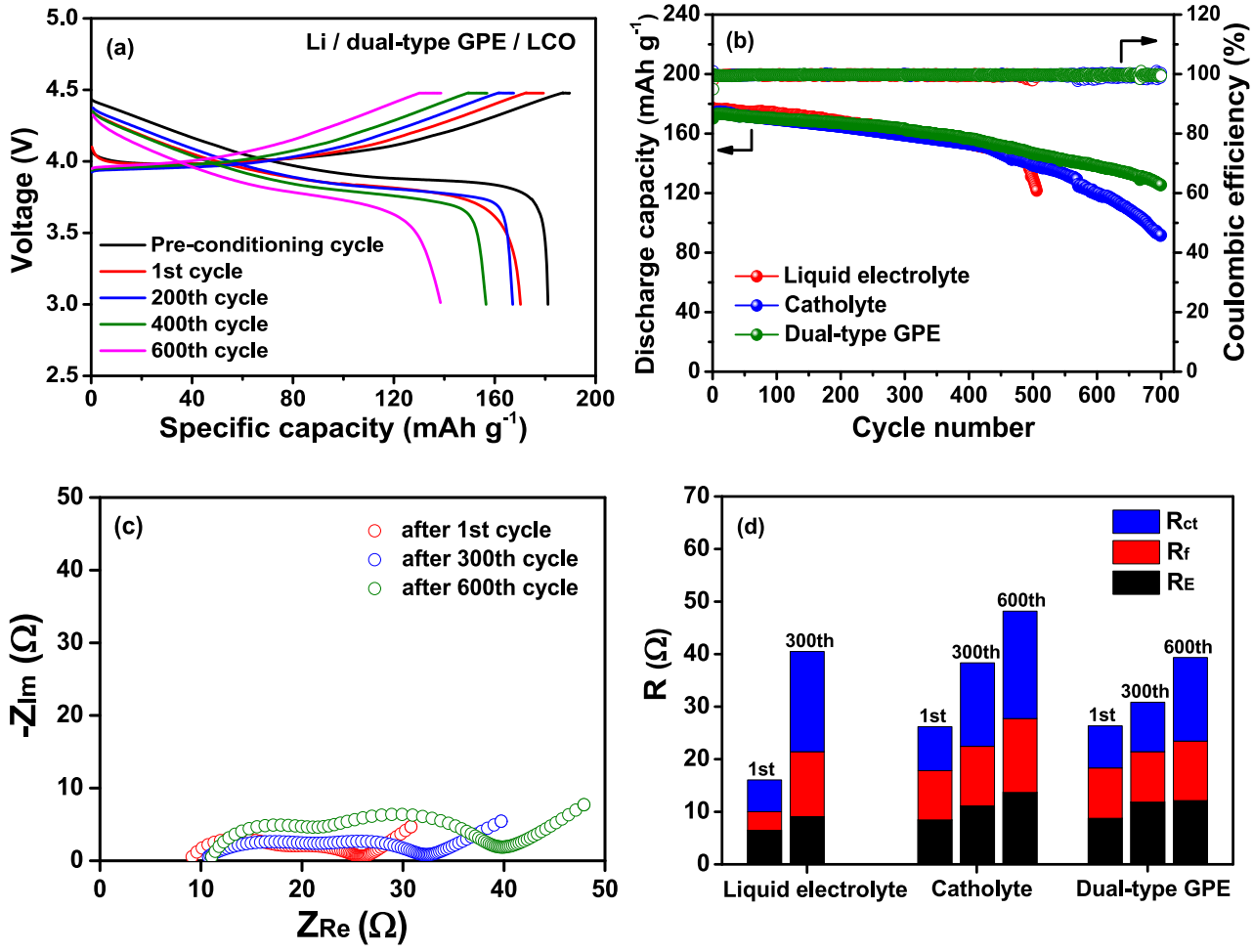

Fig. 4. (a) Voltage profiles of the Li/$LiCoO_2$ cell assembled with dual-type GPE, and (b) cycling performance of Li/$LiCoO_2$ cells with different electrolytes at 25 °C. (c) EIS plots of the Li/$LiCoO_2$ cell with dual-type GPE. (d) The values of R_E, R_f, and R_{ct} in the cells with different electrolytes at various cycle numbers.

catholyte suppressed the oxidative decomposition of the liquid electrolyte by encapsulating organic solvents in the cross-linked polymer network [25,26]. The leakage current of the Li/LCO cells was recorded to investigate the effect of the cross-linked polymer structure on oxidative stability [35]. Fig. 2f depicts the stability of the electrolyte against oxidative decomposition on the delithiated LCO cathode. The leakage current of the catholyte was lower than that of the liquid electrolyte at a constant voltage of 4.5 V, confirming the superior oxidative stability of the catholyte.

To address the issues related to lithium metal anode, an anolyte was designed to be chemically and electrochemically stable with lithium metal and to have high mechanical strength [42]. Fig. 3a and b show the optical and cross-sectional FE-SEM images of the anolyte synthesized on the lithium metal anode, respectively. The anolyte is a solid-state semi-IPN electrolyte with a thickness of 4.9 μm, as depicted in Fig. 3b. The distribution of the anolyte components was investigated using SEM and EDS elemental mapping (Fig. 3c and d). The C element arising from PEO and DVB, and the F element from LiTFSI and STFSILi were uniformly distributed in the anolyte. In addition, the mapping images of Al and Zr revealed the homogeneous dispersion of reactive alumina and LLZTO in the anolyte, which improved the mechanical strength of the anolyte. Due to the reduction in the crystallinity of PEO by adding ion-conductive LLZTO particles, the anolyte exhibited a high ionic conductivity of 3.4×10^{-6} S cm^{-1}, even in the solid state. The cross-linking reaction between the reactive alumina, DVB, and STFSILi in the anolyte was confirmed by FT-IR measurements (Fig. 3e). The reactive alumina showed the characteristic peaks associated with the asymmetric stretching vibrations of Si-O-Si at 1024 and 1176 cm^{-1}. In addition, the Si-O peak at 1302 cm^{-1} indicates the presence of Si-O-Al_2O_3 bonds [43]. The peaks observed at 1702 and 1639 cm^{-1} correspond to the stretching vibrations of C = O and C = C, respectively, in the methacrylate group of reactive alumina. In the FT-IR spectra of DVB and STFSILi, the two peaks at 1409 and 1600 cm^{-1} correspond to reactive vinyl groups (C = C) [32,33]. After the thermal cross-linking reaction, the FT-IR spectrum of the anolyte revealed that the peaks corresponding to C = C stretching vibrations in the reactive alumina, DVB, and STFSILi disappeared, suggesting that all C = C double bonds participated in free-radical polymerization to form the three-dimensional semi-IPN composite electrolyte. ^{1}H NMR spectroscopy was conducted to measure the conversion of cross-linking reaction in the anolyte, as previously reported [26,44]. As an internal standard, 1.0 wt% p-xylene was added into anolyte precursor, and the precursor was cured for different time at 70 °C. The ^{1}H NMR spectra of precursor and anolytes with different curing time are shown in Fig. 3f. The proton peaks in p-xylene can be observed at 7.04 ppm, and the peaks observed at 6.72, 5.76 and 5.25 ppm correspond to proton A, B and C in DVB and STFSILi (Fig. S5). The intensities of proton A, B and C before and after thermal curing were used to determine the reaction conversion. The peak intensities and calculated conversions are summarized in Table S2, which revealed that the reaction conversion reached 99.9 % after 5 h curing. Since we synthesized the anolyte at 70 °C for 12 h, it was plausible that the reaction conversion was almost 100 %, which is consistent with FT-IR results.

Three different electrolytes (liquid electrolyte, catholyte, and dual-type GPE) were applied to the Li/$LiCoO_2$cell, and their cycling

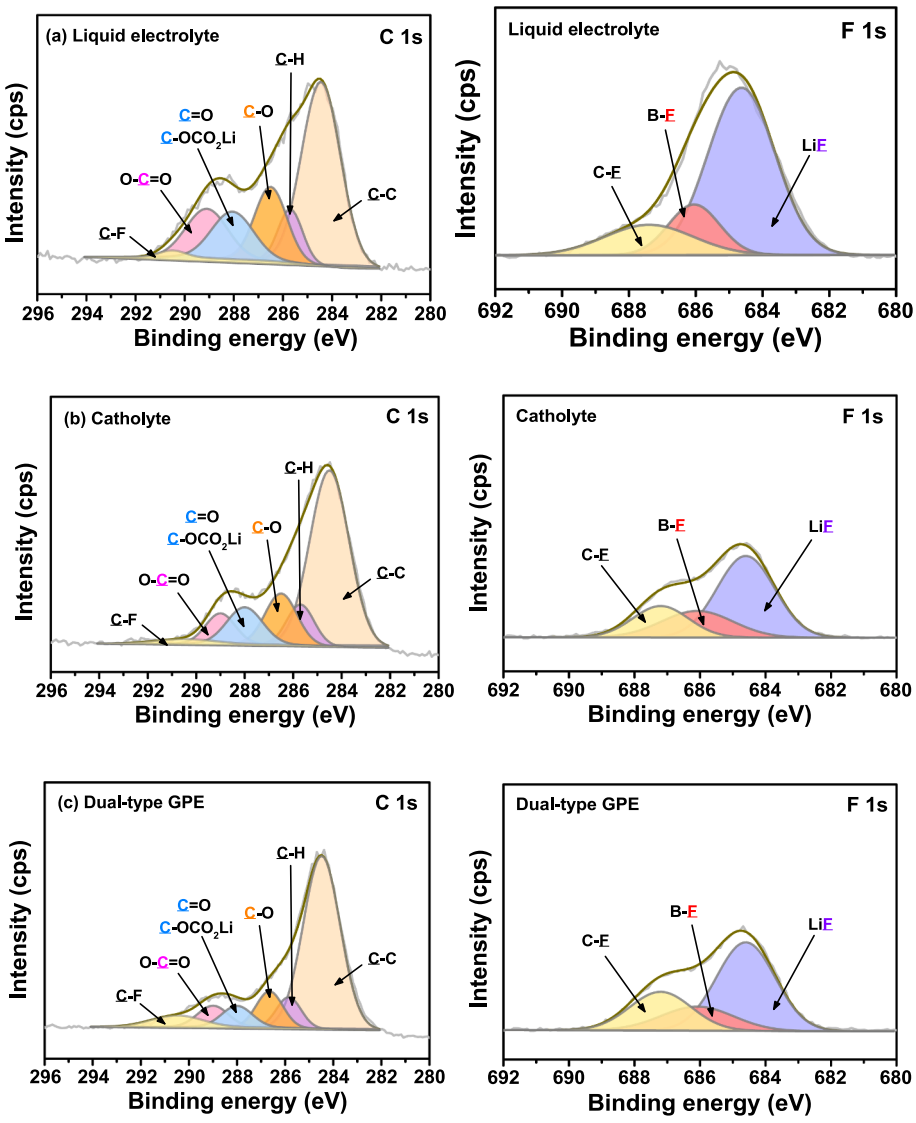

Fig. 5. XPS spectra of C 1 s and F 1 s, which were obtained from the $LiCoO_2$ cathodes cycled in the (a) liquid electrolyte, (b) catholyte, and (c) dual-type GPE after 100 cycles.

performances were evaluated. After one pre-conditioning cycle at 0.1 C rate, the cells were charged at 0.2 C and discharged at 0.5 C in the voltage range of 3.0–4.5 V to evaluate long-term cycling stability. We applied the asymmetric charge and discharge protocol with 0.2 C charge and 0.5 C discharge to minimize lithium loss during plating/stripping cycles [45]. Fig. S6a, b, and Fig. 4a show the charge and discharge curves of the Li/LCO cell employing the liquid electrolyte, catholyte, and dual-type GPE, respectively. During the pre-conditioning cycle at 0.1 C rate, the Li/LCO cell with dual-type GPE delivered a high discharge capacity of 181.1 mAh g^{-1} (Fig. 4a), corresponding to an areal capacity of 3.15 mAh cm^{-2}. For the cycling test at 0.5 C rate, the cell with the liquid electrolyte exhibited the highest initial discharge capacity of 177.0 mAh g^{-1}, however, it showed rapid capacity decay at approximately 500 cycles, resulting in cell failure (Fig. 4b). In contrast, the cells assembled with catholyte and dual-type GPE exhibited initial discharge capacities of 174.7 and 170.2 mAh g^{-1} at 0.5 C rate, respectively. The Li/LCO cell with dual-type GPE showed the highest capacity retention of 73.7 % after 700 cycles, whereas the cell with catholyte showed a capacity retention of 53.2 %. To gain further insight into the interfacial stability of the electrolytes in contact with the lithium metal anode, the AC impedance of the Li/LCO cells employing the three different electrolytes was measured before and after cycling (Fig. 4c, Fig. S7a and b). All the spectra exhibited two overlapping semicircles due to the different interfacial resistance contributions. The left semicircle in the high to middle-frequency range originates from the resistance caused by Li^+ ion migration through the film on the electrodes (R_f). The right semicircle in the middle to low-frequency range arises from the charge-transfer resistance at the electrode–electrolyte interface (R_{ct}) [46,47]. The AC impedance spectra were fitted using the equivalent circuits shown in Fig. S7c, and the results are shown in Fig. 4d. Compared to the liquid electrolyte-based cell, the cells with the catholyte and dual-type GPE initially exhibited higher resistances. However, the increase in the interfacial resistance (sum of R_f and R_{ct}) during cycling was highest in the cell employing the liquid electrolyte. Overall, the increase in the interfacial resistance was most retarded in the cell with the dual-type GPE, which can be ascribed to the synergistic effect of the anolyte and catholyte. That is, the catholyte suppressed the oxidative decomposition of the liquid electrolyte, and the anolyte inhibited the growth of a resistive layer on the lithium metal arising from deleterious reactions with liquid electrolyte, allowing the Li/LCO cell to have an excellent cycle life. We calculated energy density of the Li/$LiCoO_2$cell without considering packaging materials, according to previous work [48]. The calculated gravimetric and volumetric energy densities of the cell were 233.0 Wh kg^{-1} and 656.0 Wh L^{-1} at 25 °C, respectively. Calculation

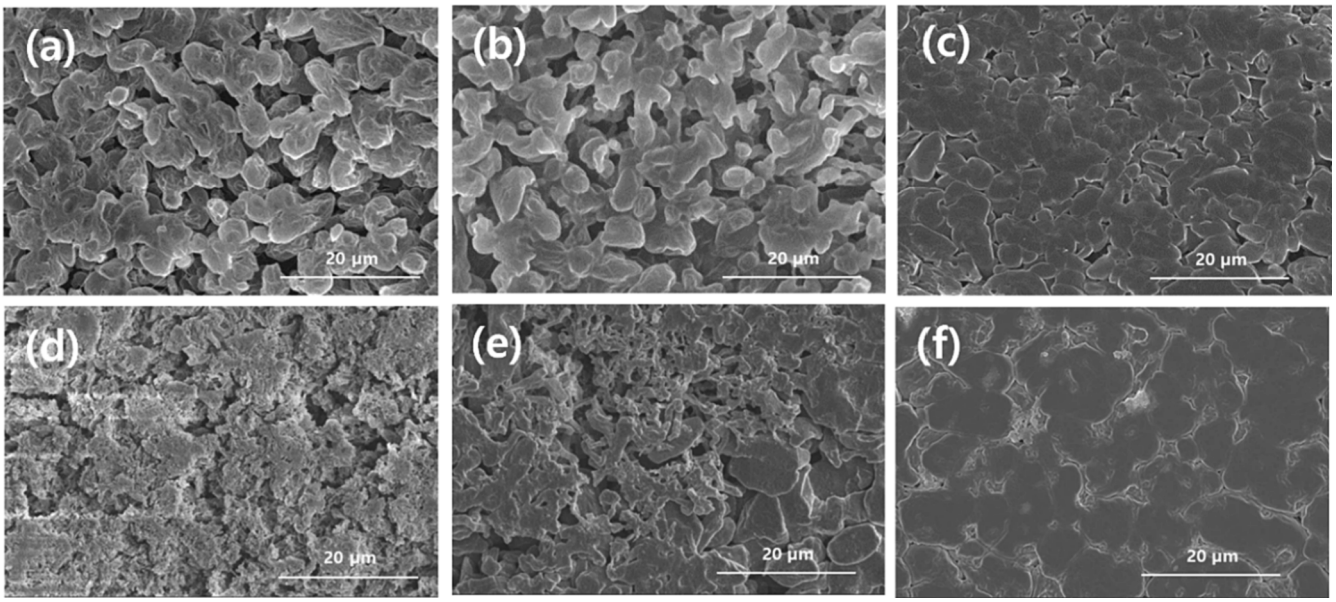

Fig. 6. SEM images of lithium metal anodes in Li/$LiCoO_2$ cells with three different electrolytes after (a–c) pre-conditioning cycle and (d–f) 100 cycles. (a), (d) Liquid electrolyte, (b), (e) catholyte, and (c), (f) dual-type GPE.

details are given in Table S3. From a practical point of view considering cycle life (700 cycles) and operating temperature (25 °C), the Li/$LiCoO_2$cell with dual-type GPE in this work exhibited high energy density when comparing with those of previous works [49,50].

XPS measurements were performed to investigate the chemical composition of the decomposition products formed on the LCO cathode, and the resulting XPS spectra are shown in Fig. 5. In the C 1 s core region, each spectrum was normalized to the intensity of the C-C peak associated with conductive carbon [16]. Two peaks at 285.8 eV (C-H) and 290.5 eV (C-F) are attributed to PVdF binder. The C 1 s spectra after cycling show additional peaks corresponding to C-O (286.5 eV), C = O/C-OCO_2Li (288.0 eV), and O-C = O (289.0 eV), which arise from the decomposition of the electrolyte components. The LCO cathodes cycled in the catholyte and dual-type GPE showed lower peak intensities for the C-O, C = O/C-OCO_2Li, and O-C = O species than the cathode cycled in the liquid electrolyte. The peak intensities in the F 1 s spectrum were normalized to those of the polymer binder (C-F) at 687.8 eV. The peaks corresponding to LiF (684.5 eV) and B-F (686.0 eV), resulting from the oxidative decomposition of FEC, $LiBF_4$, and LiDFOB [46,51], showed lower intensities in the LCO cathodes cycled in the catholyte and dual-type GPE. These results imply that the catholyte inhibits the oxidative decomposition of the electrolyte components. Fig. S8 shows the O 1 s XPS spectra of the LCO cathodes cycled in different electrolytes as a function of etching time. The intensity of the Co-O peak was significantly increased after sputtering for 20 s in the LCO cathodes in catholyte and dual-type GPE, indicating the formation of thin CEI on the LCO cathode [46,47], as schematically demonstrated in Fig. S9.

To examine the morphologies of the lithium anodes, SEM analysis of the lithium anodes cycled in different electrolytes was performed in the fully charged state (Fig. 6). After one pre-conditioning cycle, the lithium anodes cycled in the liquid electrolyte and catholyte exhibited porous structures, as shown in Fig. 6a and b. In contrast, the lithium anode cycled in the dual-type GPE exhibited a compact and dense morphology (Fig. 6c), which can be attributed to the presence of an anolyte, promoting a uniform flux of lithium ions. After 100 cycles, the lithium anodes cycled in the liquid electrolyte and catholyte exhibited moss-like lithium deposits (Fig. 6d and 6e), indicating Li dendritic growth. The growth of lithium dendrites causes the formation of a thicker SEI on the Li anode during cycling, thereby increasing the resistance of the cell and leading to a reduction in capacity. In contrast, the Li anode cycled in the dual-type GPE maintained a dense and compact morphology without dendritic Li growth (Fig. 6f), resulting in improved cycling stability (Fig. 4b). These results can be attributed to the uniform Li^+ ion flux and high mechanical strength for suppressing lithium dendrite growth, which arises from the semi-IPN-type composite anolyte consisting of ion-conductive PEO, LLZTO, and single lithium ion-conducting poly (STFSI) [52], as schematically represented in Fig. S9.

The depletion of lithium sources due to the continuous side reactions of the lithium metal and electrolyte is the primary cause of cell failure. Fig. S10a–c shows the variation in salt concentration with cycling. Salt concentration was calculated using ^1H and ^{19}F NMR analyses [53]. As depicted in Fig. S10, LiDFOB, and $LiBF_4$ were continuously consumed during the repeated charge–discharge processes. The salt depletion rate followed the order of liquid electrolyte > catholyte > dual-type GPE. The depletion behavior of LiDFOB was consistent with the cycling stability of the Li/LCO cell, demonstrating that the LiDFOB concentration is one of the most critical factors affecting the cycle life of the Li/LCO cell, as previously reported [54,55]. These results suggest that the depletion of lithium salts is the primary cause of the limited cyclability of liquid electrolyte-based cells. As represented in Fig. S10, using a dual-type GPE rather than a catholyte suppressed the salt depletion rate more effectively, indicating that the side reactions of the liquid electrolyte occurred more intensely at the lithium metal anode than at the LCO cathode.

The chemical composition of the surface layer formed on the Li anode after cycling was investigated using XPS, and the resulting spectra are shown in Fig. 7. In the C 1 s spectra, all electrolytes represented commonly observed species, such as C-C/C-H (284.7 eV), C-O (286.5 eV), R-OCO_2Li (288.0 eV), and O-C = O (289.0 eV) [56]. The lithium metal anode cycled in the dual-type GPE exhibited a significantly reduced peak intensity at 288.0 eV, which arose from the decomposition of DEC. This result indicates that introducing the anolyte on the lithium anode suppressed the side reactions between the lithium metal and the electrolyte. In the O 1 s spectra, the reaction products of lithium metal with LiDFOB and DEC were observed. The B-O moiety is formed by polymerization between the electron-deficient B atoms generated from the decomposition of LiDFOB and FEC [57,58]. The peak intensity of lithium alkoxides (RO-Li), which are the decomposition products of DEC, was substantially reduced for the lithium metal anode employing the dual-type GPE. The XPS spectra of the lithium metal anode revealed

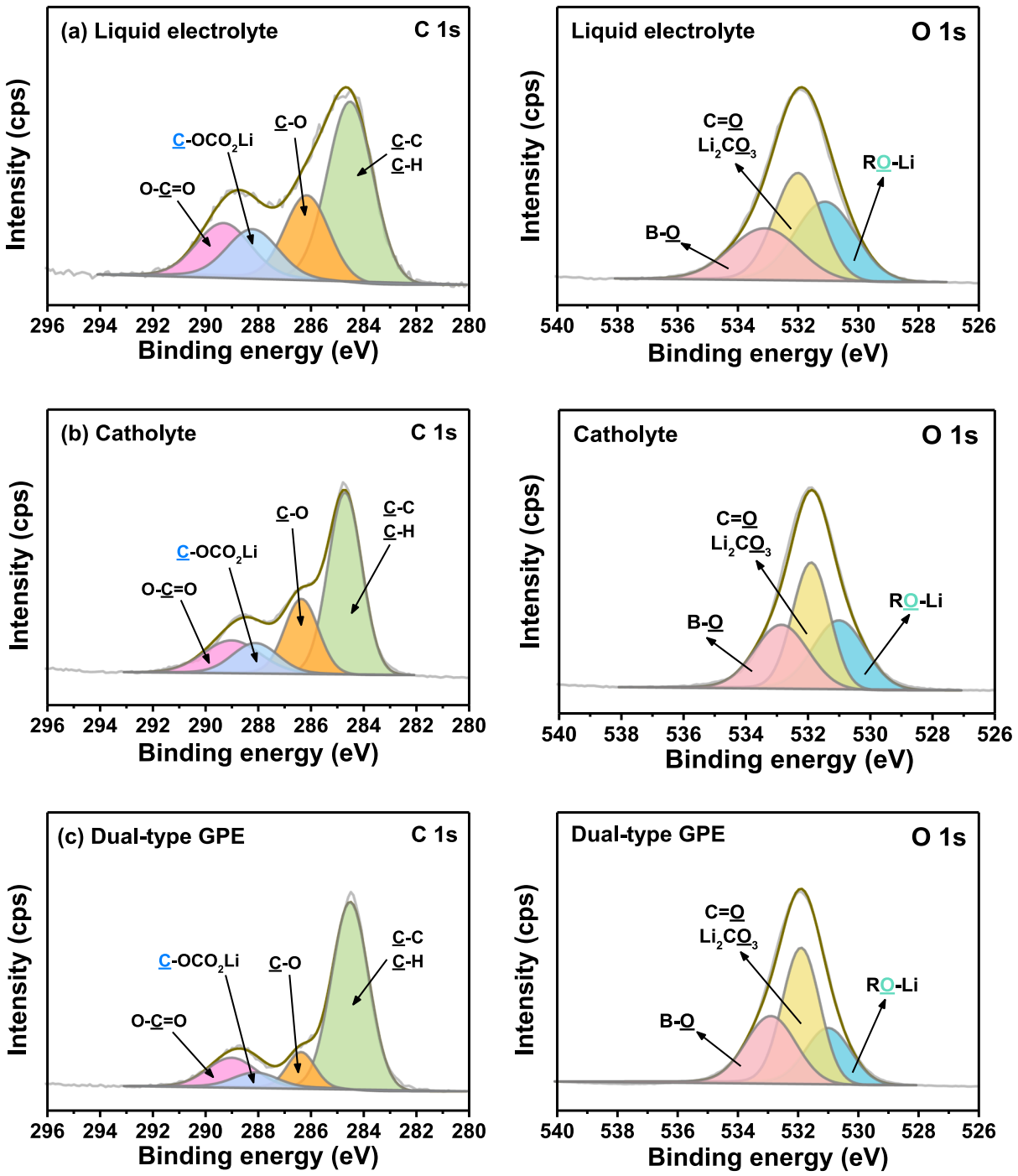

Fig. 7. XPS spectra of C 1 s and O 1 s, which were obtained from the lithium anodes cycled in the (a) liquid electrolyte, (b) catholyte, and (c) dual-type GPE after 100 cycles.

that the use of a dual-type GPE (including an anolyte) suppressed side reactions between the liquid electrolyte and lithium metal anode, which delayed the depletion of the lithium sources and improved the cycle life of the Li/LCO cells.

We evaluated the rate capability of the Li/$LiCoO_2$cells assembled with different electrolytes at 25 °C. The cell was charged to 4.5 V at 0.2 C and discharged to 3.0 V at different C rates. The cycle was repeated three times at each current rate, and the third discharge curves of the cell obtained at each C rate are presented in Fig. S11. As the current rate increased, the overpotential gradually increased with a decrease of the discharge capacity. The cell with dual-type GPE exhibited lower discharge capacity and higher polarization than the liquid electrolyte-based cell at 2.0 C rate, which can be ascribed to the higher ionic resistance of dual-type GPE. However, the cell employing catholyte delivered almost the same discharge capacity as liquid electrolyte cell at 2.0 C, which can be attributed to high t^+ value of the catholyte.

4. Conclusions

In this study, a dual-type GPE composed of an anolyte and catholyte was prepared and applied to the Li/$LiCoO_2$ cell operated at high voltage (4.5 V). A catholyte with a cross-linked structure was synthesized by the *in-situ* thermal curing of a precursor containing dual-salt liquid electrolyte and cross-linking agent, which exhibited high ionic conductivity

and superior oxidative stability above 5.0 V vs. Li/Li^+. The addition of a single Li^+-ion-conducting poly(MTFSILi) improved the Li^+-ion conductivity to a level corresponding to that of a liquid electrolyte. The anolyte, PEO-based semi-IPN composite polymer electrolyte, exhibited high ionic conductivity and mechanical properties through an appropriate combination of an ion-conductive polymer and an inorganic material. This enabled a uniform lithium-ion flux at the surface of the lithium metal anode and physically inhibited lithium dendrite growth. In addition, it suppressed side reactions between the liquid electrolyte and the lithium metal anode. Consequently, the Li/$LiCoO_2$ cell assembled with dual-type GPE exhibited a high discharge capacity of 181.1 mAh g^{-1} (areal capacity: 3.15 mAh cm^{-2}) in the voltage range of 3.0–4.5 V and an excellent cycle life with a capacity retention of 74 % after 700 cycles at 0.5 C rate due to the synergistic effect of the anolyte and catholyte.

Declaration of Competing Interest

The authors declare that they have no known competing financial interests or personal relationships that could have appeared to influence the work reported in this paper.

Data availability

Data will be made available on request.

Acknowledgments

The authors thank Samsung SDI for providing financial support.

Appendix A. Supplementary data

Supplementary data to this article can be found online at https://doi.org/10.1016/j.cej.2023.146266.

References

[1] J.M. Tarascon, M. Armand, Issues and challenges facing rechargeable lithium batteries, Nature 414 (2001) 359–367, https://doi.org/10.1038/35104644.
[2] J.B. Goodenough, K.-S. Park, The Li-Ion rechargeable battery: a perspective, J. Am. Chem. Soc. 135 (2013) 1167–1176, https://doi.org/10.1021/ja3091438.
[3] Z.P. Cano, D. Banham, S. Ye, A. Hintennach, J. Lu, M. Fowler, Z. Chen, Batteries and fuel cells for emerging electric vehicle markets, Nat. Energy 3 (2018) 279–289, https://doi.org/10.1038/s41560-018-0108-1.
[4] J. Qian, L. Liu, J. Yang, S. Li, X. Wang, H.L. Zhuang, Y. Lu, Electrochemical surface passivation of $LiCoO_2$ particles at ultrahigh voltage and its applications in lithium-based batteries, Nat. Commun. 9 (2018) 4918, https://doi.org/10.1038/s41467-018-07296-6.
[5] H.H. Sun, H.-H. Ryu, U.-H. Kim, J.A. Weeks, A. Heller, Y.-K. Sun, C.B. Mullins, Beyond doping and coating: prospective strategies for stable high-capacity layered ni-rich cathodes, ACS Energy Lett. 5 (2020) 1136–1146, https://doi.org/10.1021/acsenergylett.0c00191.
[6] W. Xue, M. Huang, Y. Li, Y.G. Zhu, R. Gao, X. Xiao, W. Zhang, S. Li, G. Xu, Y. Yu, P. Li, J. Lopez, D. Yu, Y. Dong, W. Fan, Z. Shi, R. Xiong, C.-J. Sun, I. Hwang, W.-K. Lee, Y. Shao-Horn, J.A. Johnson, J. Li, Ultra-high-voltage Ni-rich layered cathodes in practical Li metal batteries enabled by a sulfonamide-based electrolyte, Nat. Energy 6 (2021) 495–505, https://doi.org/10.1038/s41560-021-00792-y.
[7] K. Xu, Nonaqueous liquid electrolytes for lithium-based rechargeable batteries, Chem. Rev. 104 (2004) 4303–4418, https://doi.org/10.1021/cr030203g.
[8] X. Ren, L. Zou, X. Cao, M.H. Engelhard, W. Liu, S.D. Burton, H. Lee, C. Niu, B. E. Matthews, Z. Zhu, C. Wang, B.W. Arey, J. Xiao, J. Liu, J.-G. Zhang, W. Xu, Enabling high-voltage lithium-metal batteries under practical conditions, Joule. 3 (2019) 1662–1676, https://doi.org/10.1016/j.joule.2019.05.006.
[9] X.-B. Cheng, R. Zhang, C.-Z. Zhao, Q. Zhang, Toward safe lithium metal anode in rechargeable batteries: a review, Chem. Rev. 117 (2017) 10403–10473, https://doi.org/10.1021/acs.chemrev.7b00115.
[10] X. Zhang, Y. Yang, Z. Zhou, Towards practical lithium-metal anodes, Chem. Soc. Rev. 49 (2020) 3040–3071, https://doi.org/10.1039/C9CS00838A.
[11] J.-G. Zhang, W. Xu, J. Xiao, X. Cao, J. Liu, Lithium metal anodes with nonaqueous electrolytes, Chem. Rev. 120 (2020) 13312–13348, https://doi.org/10.1021/acs.chemrev.0c00275.
[12] J. Wang, B. Ge, H. Li, M. Yang, J. Wang, D. Liu, C. Fernandez, X. Chen, Q. Peng, Challenges and progresses of lithium-metal batteries, Chem. Eng. J. 420 (2021), 129739, https://doi.org/10.1016/j.cej.2021.129739.
[13] V.R. Koch, J.H. Young, 2-Methyltetrahydrofuran-Lithium hexafluoroarsenate: a superior electrolyte for the secondary lithium electrode, Science 204 (1979) 499–501, https://doi.org/10.1126/science.204.4392.499.
[14] K.M. Abraham, J.L. Goldman, D.L. Natwig, Characterization of Ether Electrolytes for Rechargeable Lithium Cells, J. Electrochem. Soc. 129 (1982) 2404, https://doi.org/10.1149/1.2123556.
[15] K. Yoshida, M. Nakamura, Y. Kazue, N. Tachikawa, S. Tsuzuki, S. Seki, K. Dokko, M. Watanabe, Oxidative-stability enhancement and charge transport mechanism in glyme-lithium salt equimolar complexes, J. Am. Chem. Soc. 133 (2011) 13121–13129, https://doi.org/10.1021/ja203983r.
[16] S. Jiao, X. Ren, R. Cao, M.H. Engelhard, Y. Liu, D. Hu, D. Mei, J. Zheng, W. Zhao, Q. Li, N. Liu, B.D. Adams, C. Ma, J. Liu, J.-G. Zhang, W. Xu, Stable cycling of high-voltage lithium metal batteries in ether electrolytes, Nat. Energy 3 (2018) 739–746, https://doi.org/10.1038/s41560-018-0199-8.
[17] S. Chen, J. Zheng, D. Mei, K.S. Han, M.H. Engelhard, W. Zhao, W. Xu, J. Liu, J. G. Zhang, High-voltage lithium-metal batteries enabled by localized high-concentration electrolytes, Adv. Mater. 30 (2018), e1706102, https://doi.org/10.1002/adma.201706102.
[18] X. Ren, S. Chen, H. Lee, D. Mei, M.H. Engelhard, S.D. Burton, W. Zhao, J. Zheng, Q. Li, M.S. Ding, M. Schroeder, J. Alvarado, K. Xu, Y.S. Meng, J. Liu, J.-G. Zhang, W. Xu, Localized high-concentration sulfone electrolytes for high-efficiency lithium-metal batteries, Chem 4 (2018) 1877–1892, https://doi.org/10.1016/j.chempr.2018.05.002.
[19] Y. Yamada, A. Yamada, Review-superconcentrated electrolytes for lithium batteries, J. Electrochem. Soc. 162 (2015) A2406, https://doi.org/10.1149/2.0041514jes.
[20] J. Moon, D.O. Kim, L. Bekaert, M. Song, J. Chung, D. Lee, A. Hubin, J. Lim, Non-fluorinated non-solvating cosolvent enabling superior performance of lithium metal negative electrode battery, Nat. Commun. 13 (2022) 4538, https://doi.org/10.1038/s41467-022-32192-5.
[21] R. Weber, M. Genovese, A.J. Louli, S. Hames, C. Martin, I.G. Hill, J.R. Dahn, Long cycle life and dendrite-free lithium morphology in anode-free lithium pouch cells enabled by a dual-salt liquid electrolyte, Nat. Energy 4 (2019) 683–689, https://doi.org/10.1038/s41560-019-0428-9.
[22] Y.-S. Lee, J.H. Lee, J.-A. Choi, W.Y. Yoon, D.-W. Kim, Cycling characteristics of lithium powder polymer batteries assembled with composite gel polymer electrolytes and lithium powder anode, Adv. Funct. Mater. 23 (2013) 1019–1027, https://doi.org/10.1002/adfm.201200692.
[23] V. Jabbari, V. Yurkiv, M.G. Rasul, M.T. Saray, R. Rojaee, F. Mashayek, R. Shahbazian-Yassar, An efficient gel polymer electrolyte for dendrite-free and long cycle life lithium metal batteries, Energy Storage Mater. 46 (2022) 352–365, https://doi.org/10.1016/j.ensm.2022.01.031.
[24] Q. Wang, X. Xu, B. Hong, M. Bai, J. Li, Z. Zhang, Y. Lai, Molecular engineering of a gel polymer electrolyte via in-situ polymerization for high performance lithium metal batteries, Chem. Eng. J. 428 (2022), 131331, https://doi.org/10.1016/j.cej.2021.131331.
[25] A. Manuel Stephan, Review on gel polymer electrolytes for lithium batteries, Eur. Polym. J. 42 (2006) 21–42, https://doi.org/10.1016/j.eurpolymj.2005.09.017.
[26] S. Park, B. Jeong, D.-A. Lim, C.H. Lee, K.H. Ahn, J.H. Lee, D.-W. Kim, Quasi-solid-state electrolyte synthesized using a thiol-ene click chemistry for rechargeable lithium metal batteries with enhanced safety, ACS Appl. Mater. Interfaces 12 (2020) 19553–19562, https://doi.org/10.1021/acsami.0c02706.
[27] S.H. Ju, Y.-S. Lee, Y.-K. Sun, D.-W. Kim, Unique core–shell structured $SiO_2(Li^+)$ nanoparticles for high-performance composite polymer electrolytes, J. Mater. Chem. A 1 (2013) 395–401, https://doi.org/10.1039/C2TA00556E.
[28] S. Choudhury, R. Mangal, A. Agrawal, L.A. Archer, A highly reversible room-temperature lithium metal battery based on crosslinked hairy nanoparticles, Nat. Commun. 6 (2015) 10101, https://doi.org/10.1038/ncomms10101.
[29] W.-K. Shin, J.H. Yoo, W. Choi, K.Y. Chung, S.S. Jang, D.-W. Kim, Cycling performance of lithium-ion polymer cells assembled with a cross-linked composite polymer electrolyte using a fibrous polyacrylonitrile membrane and vinyl-functionalized SiO_2 nanoparticles, J. Mater. Chem. A 3 (2015) 12163–12170, https://doi.org/10.1039/c5ta01436k.
[30] J.-F. Wu, Z. Zou, B. Pu, L. Ladenstein, S. Lin, W. Xie, S. Li, B. He, Y. Fan, W.K. Pang, H.M.R. Wilkening, X. Guo, C. Xu, T. Zhang, S. Shi, J. Liu, Liquid-like li-ion conduction in oxides enabling anomalously stable charge transport across the li/electrolyte interface in all-solid-state batteries, Adv. Mater. 35 (2023) 2303730, https://doi.org/10.1002/adma.202303730.
[31] Z. Xiong, Z. Wang, W. Zhou, Q. Liu, J.-F. Wu, T.-H. Liu, C. Xu, J. Liu, 4.2V polymer all-solid-state lithium batteries enabled by high-concentration PEO solid electrolytes, Energy Storage Mater. 57 (2023) 171–179, https://doi.org/10.1016/j.ensm.2023.02.008.
[32] W.-K. Shin, J. Cho, A.G. Kannan, Y.-S. Lee, D.-W. Kim, Cross-linked composite gel polymer electrolyte using mesoporous methacrylate functionalized SiO_2 nanoparticles for lithium-ion polymer batteries, Sci. Rep. 6 (2016) 26332, https://doi.org/10.1038/srep26332.
[33] H.-S. Woo, Y.-B. Moon, S. Seo, H.-T. Lee, D.-W. Kim, Semi-interpenetrating polymer network composite gel electrolytes employing vinyl-functionalized silica for lithium-oxygen batteries with enhanced cycling stability, ACS Appl. Mater. Interfaces 10 (2018) 687–695, https://doi.org/10.1021/acsami.7b15573.
[34] P.G. Bruce, J. Evans, C.A. Vincent, Conductivity and transference number measurements on polymer electrolytes, Solid State Ion. 28–30 (1988) 918–922, https://doi.org/ 10.1016/0167-2738(88)90304-9.
[35] Y. Li, G.M. Veith, K.L. Browning, J. Chen, D.K. Hensley, M.P. Paranthaman, S. Dai, X.-G. Sun, Lithium malonatoborate additives enabled stable cycling of 5V lithium

metal and lithium ion batteries, Nano Energy 40 (2017) 9–19, https://doi.org/10.1016/j.nanoen.2017.07.051.
[36] L. Chen, Y. Li, S.-P. Li, L.-Z. Fan, C.-W. Nan, J.B. Goodenough, PEO/garnet composite electrolytes for solid-state lithium batteries: From "ceramic-in-polymer" to "polymer-in-ceramic", Nano Energy 46 (2018) 176–184, https://doi.org/10.1016/j.nanoen.2017.12.037.
[37] J.J. Lu, Y. Liu, P. Yao, Z. Ding, Q. Tang, J. Wu, Z. Ye, K. Huang, X. Liu, Hybridizing poly(vinylidene fluoride-co-hexafluoropropylene) with $Li_{6.5}La_3Zr_{1.5}Ta_{0.5}O_{12}$ as a lithium-ion electrolyte for solid state lithium metal batteries, Chem. Eng. J. 367 (2019) 230–238, https://doi.org/10.1016/j.cej.2019.02.148.
[38] S. Kim, J. Ryu, J. Rim, D. Hong, J. Kang, S. Park, Vinyl-integrated in situ cross-linked composite gel electrolytes for stable lithium metal anodes, ACS Appl. Energy Mater. 4 (2021) 2922–2931, https://doi.org/10.1021/acsaem.1c00327.
[39] E. Quartarone, P. Mustarelli, Electrolytes for solid-state lithium rechargeable batteries: recent advances and perspectives, Chem. Soc. Rev. 40 (2011) 2525–2540, https://doi.org/10.1039/C0CS00081G.
[40] M.-S. Park, H.-S. Woo, J.-M. Heo, J.-M. Kim, R. Thangavel, Y.-S. Lee, D.-W. Kim, Thermoplastic polyurethane elastomer-based gel polymer electrolytes for sodium-metal cells with enhanced cycling performance, ChemSusChem 12 (2019) 4645–4654, https://doi.org/10.1002/cssc.201901799.
[41] E.J. Olson, P. Buhlmann, Unbiased assessment of electrochemical windows: minimizing mass transfer effects on the evaluation of anodic and cathodic limits, J. Electrochem. Soc. 160 (2013) A320, https://doi.org/10.1149/2.068302jes.
[42] H. Zhou, S. Yu, H. Liu, P. Liu, Protective coatings for lithium metal anodes: Recent progress and future perspectives, J. Power Sources. 450 (2020) 227632, https://doi.org/ 10.1016/ j.jpowsour.2019.227632.
[43] F. Kundie, C. Azhari, Z. Ahmad, Effect of nano- and micro-alumina fillers on some properties of poly(methyl methacrylate) denture base composites, J. Serb. Chem. Soc. 83 (2017) 56, https://doi.org/10.2298/JSC170118056K.
[44] J.H. Ahn, H.-M. Kim, Y.-J. Lee, D. Esken, D. Dehe, H.A. Song, D.-W. Kim, Nanostructured reactive alumina particles coated with water-soluble binder on the polyethylene separator for highly safe lithium-ion batteries, J. Power Sources 506 (2021), 230119, https://doi.org/10.1016/j.jpowsour.2021.230119.
[45] A.J. Louli, M. Coon, M. Genovese, J. deGooyer, A. Eldesoky, J.R. Dahn, Optimizing Cycling Conditions for Anode-Free Lithium Metal Cells, J. Electrochem. Soc. 168 (2021) 020515, https://doi.org/10.1149/1945-7111/abe089.
[46] J. Li, W. Li, Y. You, A. Manthiram, Extending the service life of high-ni layered oxides by tuning the electrode-electrolyte interphase, Adv. Energy Mater. 8 (2018) 1801957, https://doi.org/10.1002/aenm.201801957.
[47] L.D. Ellis, I.G. Hill, K.L. Gering, J.R. Dahn, Synergistic effect of $LiPF_6$ and $LiBF_4$ as electrolyte salts in lithium-ion cells, J. Electrochem. Soc. 164 (2017) A2426, https://doi.org/10.1149/2.0811712jes.
[48] J.-H. Kim, J.-M. Kim, S.-K. Cho, N.-Y. Kim, S.-Y. Lee, Redox-homogeneous, gel electrolyte-embedded high-mass-loading cathodes for high-energy lithium metal batteries, Nat. Commun. 13 (2022) 2541, https://doi.org/10.1038/s41467-022-30112-1.
[49] R. Sahore, Z. Du, X.C. Chen, W.B. Hawley, A.S. Westover, N.J. Dudney, Practical considerations for testing polymer electrolytes for high-energy solid-state batteries, ACS Energy Lett. 6 (2021) 2240–2247, https://doi.org/10.1021/acsenergylett.1c00810.
[50] R. Sahore, G. Yang, X.C. Chen, W.-Y. Tsai, J. Li, N.J. Dudney, A. Westover, A bilayer electrolyte design to enable high-areal-capacity composite cathodes in polymer electrolytes based solid-state lithium metal batteries, ACS Appl. Energy Mater. 5 (2022) 1409–1413, https://doi.org/10.1021/acsaem.2c00050.
[51] F. Ding, W. Xu, X. Chen, J. Zhang, M.H. Engelhard, Y. Zhang, B.R. Johnson, J. V. Crum, T.A. Blake, X. Liu, J.-G. Zhang, Effects of carbonate solvents and lithium salts on morphology and coulombic efficiency of lithium electrode, J. Electrochem. Soc. 160 (2013) A1894, https://doi.org/10.1149/2.100310jes.
[52] S.-H. Kim, K.-H. Choi, S.-J. Cho, E.-H. Kil, S.-Y. Lee, Mechanically compliant and lithium dendrite growth-suppressing composite polymer electrolytes for flexible lithium-ion batteries, J. Mater. Chem. A 1 (2013) 4949–4955, https://doi.org/10.1039/C3TA10612H.
[53] A.J. Louli, A. Eldesoky, J. deGooyer, M. Coon, C.P. Aiken, Z. Simunovic, M. Metzger, J.R. Dahn, Different Positive Electrodes for Anode-Free Lithium Metal Cells, J. Electrochem. Soc. 169 (2022), 040517, https://doi.org/10.1149/1945-7111/ac62c4.
[54] A.J. Louli, A. Eldesoky, R. Weber, M. Genovese, M. Coon, J. deGooyer, Z. Deng, R. T. White, J. Lee, T. Rodgers, R. Petibon, S. Hy, S.J.H. Cheng, J.R. Dahn, Diagnosing and correcting anode-free cell failure via electrolyte and morphological analysis, Nat. Energy 5 (2020) 693–702, https://doi.org/10.1038/s41560-020-0668-8.
[55] C. Niu, H. Lee, S. Chen, Q. Li, J. Du, W. Xu, J.-G. Zhang, M.S. Whittingham, J. Xiao, J. Liu, High-energy lithium metal pouch cells with limited anode swelling and long stable cycles, Nat. Energy 4 (2019) 551–559, https://doi.org/10.1038/s41560-019-0390-6.
[56] J. Wu, Z. Rao, X. Liu, Y. Shen, C. Fang, L. Yuan, Z. Li, W. Zhang, X. Xie, Y. Huang, Polycationic polymer layer for air-stable and dendrite-free li metal anodes in carbonate electrolytes, Adv. Mater. 33 (2021) 2007428, https://doi.org/10.1002/adma.202007428.
[57] S. Li, Q. Liu, W. Zhang, L. Fan, X. Wang, X. Wang, Z. Shen, X. Zang, Y. Zhao, F. Ma, Y. Lu, High-efficacy and polymeric solid-electrolyte interphase for closely packed li electrodeposition, Adv. Sci. 8 (2021) 2003240, https://doi.org/10.1002/advs.202003240.
[58] J. Cha, J.-G. Han, J. Hwang, J. Cho, N.-S. Choi, Mechanisms for electrochemical performance enhancement by the salt-type electrolyte additive, lithium difluoro (oxalato)borate, in high-voltage lithium-ion batteries, J. Power Sources 357 (2017) 97–106, https://doi.org/10.1016/j.jpowsour.2017.04.094.